

The evaluating study of the momentum and heat exchange process of two surface layer schemes during the severe haze pollution in Jing-Jin-Ji in east China

Yue Peng^{1,2}, Hong Wang^{1,2}, Yubin Li³, Changwei Liu³, Tianliang Zhao², Xiaoye Zhang¹, Zhiqiu Gao^{3,4}, Tong Jiang⁵, Huizheng Che¹, Meng Zhang⁶

¹ State Key Laboratory of Severe Weather/Institute of Atmospheric Composition, Chinese Academy of Meteorological Sciences (CMAS), Beijing 100081, China

² Collaborative Innovation Center on Forecast and Evaluation of Meteorological Disasters/Key Laboratory for Aerosol-Cloud-Precipitation of China Meteorological Administration, Nanjing University of Information Science and Technology, Nanjing 210044, China

³ Key Laboratory of Meteorological Disaster of Ministry of Education/Collaborative Innovation Center on Forecast and Evaluation of Meteorological Disasters, School of Remote Sensing and Geomatics Engineering, Nanjing University of Information Science and Technology, Nanjing 210044, China

⁴ State Key Laboratory of Atmospheric Boundary Layer Physics and Atmospheric Chemistry, Institute of Atmospheric Physics, Chinese Academy of Sciences, Beijing 100029, China

⁵ National Climate Center, China Meteorological Administration, Beijing 100081, China

⁶ Beijing Meteorological Service, Beijing 100089, China

Correspondence to: Hong Wang (wangh@cma.gov.cn)

Abstract. The turbulent flux parameterization schemes in surface layer are crucial for air pollution modeling. The pollutants prediction by atmosphere chemical model exist obvious deficiencies, which may be closely related to the uncertainties of the momentum and sensible heat fluxes calculated in the surface layer. The differences of two surface layer schemes (the Li and MM5 scheme) were discussed and the performance of the two schemes was evaluated based on the observed momentum and sensible heat fluxes in Jing-Jin-Ji in east China. The results showed that the aerodynamic roughness length z_{0m} and the thermal roughness length z_{0h} play an important role in the flux calculation. Compared with the Li scheme, ignoring the difference between the two in the MM5 scheme induced great error in the calculation of sensible heat flux (e.g., the error was 54% at Gucheng station). Besides the roughness lengths, the algorithms of universal functions as well as the roughness sublayer also resulted in certain errors in the MM5 scheme. In addition, the magnitudes of z_{0m} and z_{0h} have significant influence on the two schemes. The large z_{0m} and z_{0m}/z_{0h} in megacity with rough surface (e.g., Beijing) resulted in much larger differences of momentum and sensible heat fluxes by Li and MM5, compared with the small z_{0m} and z_{0m}/z_{0h} in suburban area with smooth surface (e.g., Gucheng). The Li scheme better characterized the evolution of atmospheric stratification than the MM5 scheme in general, especially for the transition stage from unstable to stable atmospheric stratification corresponding to the $PM_{2.5}$ accumulation. The bias of momentum and sensible heat fluxes from Li were lower about 38% and 43% respectively than those from MM5 during this stage. This study indicates the superiority of the Li scheme in the describing of the regional atmospheric stratification, and also suggests the improving possibility of severe haze

35 prediction in Jing-Jin-Ji in east China by coupling it into the atmosphere chemical model online.

36 **Key words:** surface layer; turbulent flux parameterization; roughness length; numerical modeling; air pollution

37 **1 Introduction**

38 Adequate air quality modeling relies on accurate simulations of meteorological conditions, especially in planetary
39 boundary layer (PBL) (Hu et al., 2010; Cheng et al., 2012; Xie et al., 2012). The PBL is closely coupled to the earth's surface
40 by turbulent exchange processes. As the bottom layer of PBL, the surface layer (SL) reflects the surface state by calculating
41 momentum, heat, water vapor and other fluxes, and influences the atmospheric structure by turbulent transport process.
42 Many studies have illustrated the important roles of meteorological factors in the SL in the formation of air pollution. They
43 demonstrated that weak wind speed, high relative humidity (RH) and strong temperature inversion are favorable for the haze
44 concentrating (Zhang et al., 2014; Yang et al., 2015; Liu et al., 2017; Zhong et al., 2017). The strong stable stratification and
45 weak turbulent are mainly responsible for many haze events. The relationship between flux and atmospheric profile in the
46 atmospheric surface layer is a key factor for air pollution diffusion, especially under stable stratification conditions (Li et al.,
47 2017). However, the study of stable boundary layer still has some uncertainties due to the poor description of surface
48 turbulent motion. The simulating study on a severe haze in east China by the Weather Research and Forecasting/Chemistry
49 (WRF-Chem) model concluded that there is lower ability of current PBL schemes in distinguishing the diffusion between
50 haze days under stable condition and clean days under unstable condition (Li et al., 2016a). Another study (Vautard et al.
51 2012) on mesoscale meteorological models also pointed out a systematic overestimation of near-surface wind speed in a
52 stable boundary layer and its possible contribution to the underestimation of the PM_{2.5} pollution. In addition,
53 atmospheric conditions in both the PBL and upper layers are strongly dependent on the turbulent fluxes which are computed
54 in the SL (Ban et al., 2010). Flux parameterization in the SL plays an important role in studies of the hydrological cycle and
55 weather prediction (Yang et al., 2001; Li, 2014). An adequate SL scheme is crucial to provide an accurate atmospheric
56 evolution by numerical models (Jiménez et al., 2012) and hence it may introduce important impacts on air pollution
57 simulation.

58 The bulk aerodynamic formulation based on Monin-Obukhov similarity theory (hereinafter MOST, Monin and
59 Obukhov, 1954) is usually employed to calculate surface fluxes in numerical models. Turbulent fluxes are parameterized by
60 wind, temperature, humidity in the lowest layer in model and temperature and humidity in surface. Many international
61 scholars verified the MOST using of field experiments and then proposed the universal functions, the commonly used of
62 which is Businger-Dyer (BD) equation (Businger, 1966; Dyer, 1967). With the development of observation technology, the
63 coefficients in the BD equation have been further modified (Paulson, 1970; Webb, 1970; Businger et al., 1971; Dyer, 1974;
64 Högström, 1996). In addition to the BD equation, some other schemes have been put forward and they performed better

65 especially for the strongly stable stratification (Holtslag and De Bruin, 1988; Beljaars and Holtslag, 1991; Cheng and
66 Brutsaert, 2005). The schemes can be divided into two types according to the computing characteristics. One type is called as
67 iterative algorithm (Paulson, 1970; Businger et al., 1971; Dyer, 1974; Högström, 1996; Beljaars and Holtslag, 1991), and it
68 keeps the MOST completely with less approximation so that the results can be more precise. However, it needs to take much
69 more steps to converge and hence the CPU time is consuming which reduces the computational efficiency of modeling
70 (Louis, 1979; Li et al., 2014); The other one is called as non-iterative algorithm (Louis et al., 1982; Launiainen, 1995; Wang
71 et al., 2002; Wouters et al., 2012). There is no need for loop iteration in the calculation due to the approximate treatment.
72 This algorithm is much simpler and less CPU time-consuming, but the results are based on the loss of the calculation
73 accuracy.

74 A new non-iterative scheme proposed by Li et al. (2014; 2015, Li hereinafter) speeds up effectively under a higher
75 accuracy compared with some classic iterative computation. It is remarkable that this new scheme just have been
76 theoretically evaluated and it has never been applied in any models. Haze pollution occurs frequently in recent years in east
77 China. The concentration of $PM_{2.5}$ may reach up to $1000 \mu g \cdot m^{-3}$ in the Beijing-Tianjin-Hebei (Jing-Jin-Ji) region in
78 winter (Wang et al., 2014) while it was generally underestimated by current air quality models (Zhang et al., 2015; Li et al.,
79 2016a; Liu et al., 2017). The Li and another classic SL scheme (Zhang and Anthes, 1982, MM5 hereinafter) are compared in
80 details in this study. The observed momentum and sensible heat flux data covering once complete haze process at Gucheng
81 station was used to evaluate the two schemes focusing on the transition stage from unstable to stable atmospheric stratification
82 corresponding to the $PM_{2.5}$ accumulation. The evaluation is in the view of both local and regional scales. This offline study
83 may provide the prerequisite for the online coupling the Li scheme into atmosphere chemical model in the future.

84 **2 Theory**

85 The definition of the momentum and sensible heat flux as well as the detailed algorithms of the Li and MM5 schemes
86 are introduced in this section.

87 **2.1 Introduction of the momentum and sensible heat flux**

88 The turbulent fluxes from ground surface are defined as follows:

$$89 \tau = \rho u_*^2, \quad (1a)$$

$$90 H = -\rho c_p u_* \theta_*. \quad (1b)$$

91 Where τ is the momentum flux, H is the sensible heat flux, ρ is the air density, c_p is the specific heat capacity at
92 constant pressure. u_* and θ_* are the friction velocity and the temperature scale respectively, and they represent the
93 intensity of the vertical turbulent flux transport and they are approximately independent on height in the SL.

94 Both the Li and MM5 schemes are calculated with bulk flux parameterization. As an important dimensionless parameter

95 related to the stability, the bulk Richardson number Ri_B is defined as

$$96 \quad Ri_B = \frac{gz(\theta - \theta_g)}{\theta u^2}. \quad (2)$$

97 Where g is the acceleration of gravity, z is the reference height which is the lowest level in the model, θ is the mean
 98 potential temperature at height z , θ_g is the surface radiometric potential temperature, u is the mean wind speed at height z .
 99 Thus, Ri_B can be computed through meteorological variables at least two levels.

100 2.2 The Li scheme

101 This new scheme employ non-iterative algorithm to compute the surface fluxes. Its basic idea is to parameterize the
 102 stability parameter ζ directly with Ri_B and roughness lengths (z_{0m} and z_{0h}). Specifically, bulk transfer coefficients of the
 103 momentum and sensible heat fluxes (C_M and C_H) are expressed as

$$104 \quad C_M = \frac{u_*^2}{u^2} = \frac{\tau}{\rho u^2}, \quad (3a)$$

$$105 \quad C_H = \frac{u_* \theta_*}{u(\theta - \theta_g)} = -\frac{H}{\rho c_p u(\theta - \theta_g)}. \quad (3b)$$

106 Based on MOST and considering the roughness sublayer (RSL) effect at the same time, the relationship between the
 107 bulk transfer coefficients and the profile functions corresponding to wind and potential temperature are usually expressed as

$$108 \quad C_M = \frac{k^2}{\left[\ln \frac{z}{z_{0m}} - \psi_M\left(\frac{z}{L}\right) + \psi_M\left(\frac{z_{0m}}{L}\right) + \psi_M^*\left(\frac{z}{L}, \frac{z}{z_*}\right) \right]^2}, \quad (4a)$$

$$109 \quad C_H = \frac{k^2}{R \left[\ln \frac{z}{z_{0m}} - \psi_M\left(\frac{z}{L}\right) + \psi_M\left(\frac{z_{0m}}{L}\right) + \psi_M^*\left(\frac{z}{L}, \frac{z}{z_*}\right) \right] \left[\ln \frac{z}{z_{0h}} - \psi_H\left(\frac{z}{L}\right) + \psi_H\left(\frac{z_{0h}}{L}\right) + \psi_H^*\left(\frac{z}{L}, \frac{z}{z_*}\right) \right]}. \quad (4b)$$

110 Where k is the von Kármán constant which is 0.4 in both two schemes, R is the Prandtl number which is 1.0 in the
 111 two schemes, z_{0m} and z_{0h} are the aerodynamic roughness length and the thermal roughness length, respectively. ψ_M and
 112 ψ_H are the integrated stability functions for momentum and sensible heat, respectively, which are also called universe
 113 functions. L is the Obukhov length ($\zeta = \frac{z}{L}$), ψ_M^* and ψ_H^* are the correction functions accounting for RSL effect, z_* is the
 114 RSL height. It is clear to see that the calculation of the momentum and sensible heat fluxes requires C_M and C_H (or u_* and
 115 θ_*), and there are 3 key points to get them:

116 1. z_{0m} and z_{0h} . z_{0m} and z_{0h} are two key parameters in the bulk transfer equations. Their definitions and influence
 117 will be discussed in Sect. 4.1. Note that both z_{0m} and z_{0h} are taken into account by the Li scheme. In other words,
 118 the Li scheme distinguishes these two important surface parameters effectively as they generate from different
 119 mechanisms.

120 2. ζ . The determination of ζ is the most crucial problem for the Li scheme. In fact, this new scheme includes two
 121 parts. The first part was proposed for atmospheric stable stratification condition (Li et al., 2014), and the second part
 122 then extended the scheme to unstable condition (Li et al., 2015). For stable condition, the calculation procedure for a
 123 given group of Ri_B , z_{0m} and z_{0h} is the following: (1) find the region according to z_{0m} and z_{0h} ; (2) find the section

124 according to the region and Ri_B with Eq. (5) and given coefficients; (3) calculate ζ using Eq. (6) and given
 125 coefficients.

$$126 \quad Ri_{Bcp} = \sum C_{mn} (\log L_{0M})^m (L_{0H} - L_{0M})^n, \quad (5)$$

$$127 \quad \zeta = Ri_B \sum C_{ijk} Ri_B^i L_{0M}^j (L_{0H} - L_{0M})^k. \quad (6)$$

128 Where C_{mn} and C_{ijk} are the coefficients in Tables in Li et al. (2014). $L_{0M} = \ln \frac{z}{z_{0m}}$, $L_{0H} = \ln \frac{z}{z_{0h}}$. $m, n =$
 129 $0, 1, 2$, and $m + n \leq 3$; $i, j, k = 0, 1, 2, 3$, and $i + j + k \leq 4$. Similarly, for unstable condition, eight regions are
 130 divided according to the method from Li et al. (2015). For each of the regions, ζ is carried out by following:

$$131 \quad \zeta = Ri_B \frac{L_{0M}^2}{L_{0H}} \sum C_{ijk} \left(\frac{-Ri_B}{1-Ri_B} \right)^i L_{0M}^{-j} L_{0H}^{-k}. \quad (7)$$

132 Where C_{ijk} is listed in Li et al. (2016b), and $i = 0, 1$; $j, k = 0, 1, 2, 3$; $i + j + k \leq 4$.

133 3. Universal function. It is also a key factor in flux calculation. The form of universal function here is adopted from
 134 Cheng and Brutsaert (2005) under the stable condition (Eqs. (8a), (8b)) and it is adopted from Paulson (1970) under the
 135 unstable condition (Eqs. (9a), (9b)):

$$136 \quad \psi_M(\zeta) = -a \ln \left[\zeta + (1 + \zeta^b)^{\frac{1}{b}} \right], \quad \zeta > 0 \text{ (stable)}, \quad (8a)$$

$$137 \quad \psi_H(\zeta) = -c \ln \left[\zeta + (1 + \zeta^d)^{\frac{1}{d}} \right], \quad \zeta > 0 \text{ (stable)}, \quad (8b)$$

$$138 \quad \psi_M(\zeta) = 2 \ln \frac{1+x}{2} + \ln \frac{1+x^2}{2} - 2 \arctan(x) + \frac{\pi}{2}, \quad \zeta < 0 \text{ (unstable)}, \quad (9a)$$

$$139 \quad \psi_H(\zeta) = 2 \ln \frac{1+y}{2}, \quad \zeta < 0 \text{ (unstable)}. \quad (9b)$$

140 Where $a = 6.1$, $b = 2.5$, $c = 5.3$, $d = 1.1$, $x = (1 - 16\zeta)^{1/4}$, $y = (1 - 16\zeta)^{1/2}$.

141 In addition, the RSL effect is taken into account in the Li scheme. The definitions and influence of RSL will also be
 142 discussed in Sect. 4.1. De Ridder (2010) proposed the expression of ψ_M^* and ψ_H^* :

$$143 \quad \psi_M^* \left(\zeta, \frac{z}{z_*} \right) = \phi_M \left[\left(1 + \frac{v}{\mu_M z / z_*} \right) \zeta \right]^{\frac{1}{\lambda}} \ln \left(1 + \frac{\lambda}{\mu_M z / z_*} \right) e^{-\mu_M z / z_*}, \quad (10a)$$

$$144 \quad \psi_H^* \left(\zeta, \frac{z}{z_*} \right) = \phi_H \left[\left(1 + \frac{v}{\mu_H z / z_*} \right) \zeta \right]^{\frac{1}{\lambda}} \ln \left(1 + \frac{\lambda}{\mu_H z / z_*} \right) e^{-\mu_H z / z_*}. \quad (10b)$$

145 Where $v = 0.5$, $\mu_M = 2.59$, $\mu_H = 0.95$, $z_* = 16.7 z_{0m}$, $\lambda = 1.5$. ϕ_M and ϕ_H are universal functions before
 146 integration. Here, set $\chi_M = 1 + \frac{v}{\mu_M z / z_*}$, $\chi_H = 1 + \frac{v}{\mu_H z / z_*}$:

$$147 \quad \phi_M(\chi_M \zeta) = 1 + a \frac{\chi_M \zeta + (\chi_M \zeta)^b [1 + (\chi_M \zeta)^b]^{\frac{1-b}{b}}}{\chi_M \zeta + [1 + (\chi_M \zeta)^b]^{\frac{1}{b}}}, \quad \zeta > 0 \text{ (stable)}, \quad (11a)$$

$$148 \quad \phi_H(\chi_H \zeta) = 1 + c \frac{\chi_H \zeta + (\chi_H \zeta)^d [1 + (\chi_H \zeta)^d]^{\frac{1-d}{d}}}{\chi_H \zeta + [1 + (\chi_H \zeta)^d]^{\frac{1}{d}}}, \quad \zeta > 0 \text{ (stable)}, \quad (11b)$$

$$149 \quad \phi_M(\chi_M \zeta) = (1 - 16\chi_M \zeta)^{-1/4}, \quad \zeta < 0 \text{ (unstable)}, \quad (12a)$$

150
$$\phi_H(\chi_H \zeta) = (1 - 16\chi_H \zeta)^{-1/2}, \quad \zeta < 0 \text{ (unstable)}. \quad (12b)$$

151 **2.3 The MM5 scheme**

152 The MM5 scheme is a classic one which is widely applied in modeling investigation (Hu et al., 2010; Wang et al.,
 153 2015a, b; Tymvios et al., 2017). This scheme dose not distinguish z_{0h} from z_{0m} , thus the roughness length here is
 154 expressed as z_0 . For unstable condition, the function forms are given by Eqs. (16a) and (16b) following Paulson (1970), and
 155 for stable condition, the atmospheric stratification conditions are subdivided into three cases according to Zhang and Anthes
 156 (1982) and the function forms are given by Eqs. (13), (14), and (15).

157 (1) Strongly stable condition ($Ri_B \geq 0.2$):

158
$$\psi_M = \psi_H = -10 \ln \frac{z}{z_0}. \quad (13)$$

159 (2) Weakly stable condition ($0 < Ri_B < 0.2$):

160
$$\psi_M = \psi_H = -5 \left(\frac{Ri_B}{1.1 - 5Ri_B} \right) \ln \frac{z}{z_0}. \quad (14)$$

161 (3) Neutral condition ($Ri_B = 0$):

162
$$\psi_M = \psi_H = 0. \quad (15)$$

163 (4) Unstable condition ($Ri_B < 0$):

164
$$\psi_M = 2 \ln \frac{1+x}{2} + \ln \frac{1+x^2}{2} - 2 \arctan(x) + \frac{\pi}{2}, \quad (16a)$$

165
$$\psi_H = 2 \ln \frac{1+y}{2}, \quad (16b)$$

166 where $x = (1 - 16\zeta)^{1/4}$, $y = (1 - 16\zeta)^{1/2}$.

167 This scheme calculates turbulent fluxes of the momentum and sensible heat with u_* and θ_* . In order to avoid the huge
 168 difference of u_* through the two computation, u_* is arithmetically averaged with its previous value with Eq. (17), and a
 169 lower limit of $u_* = 0.1$ m/s is imposed to prevent the heat flux from being zero under very stable conditions. According to
 170 the profile functions of wind and temperature near the ground, θ_* then is deduced by Eq. (18).

171
$$u_* = \frac{1}{2} \left(u_* + \frac{ku}{\ln \frac{z}{z_{0m}} - \psi_M} \right), \quad (17)$$

172
$$\theta_* = \frac{k(\theta - \theta_g)}{R[\ln \frac{z}{z_{0h}} - \psi_H]}. \quad (18)$$

173 The calculation procedure of the Li scheme is the following: (1) determine Ri_B 、 z_{0m} and z_{0h} according to the
 174 observation data; (2) calculate ζ with Ri_B 、 z_{0m} and z_{0h} ; (3) calculate the momentum and sensible heat fluxes under
 175 different conditions. The MM5 scheme is summarized as follows: (1) determine the universal functions according to the
 176 values of Ri_B and z_0 ; (2) calculate the u_* and θ_* with the meteorological variables and flux data; (3) derive the turbulent
 177 fluxes. Compared with other non-iterative schemes including MM5, the Li scheme can be applied to the full range of

178 roughness status $10 \leq \frac{z}{z_{0m}} \leq 10^5$ and $-0.5 \leq \ln \frac{z_{0m}}{z_{0h}} \leq 30$ under whole conditions $-5 \leq Ri_B \leq 2.5$. In addition, there are
179 three obvious differences between the Li and MM5 schemes: (1) Li distinguishes z_{0h} from z_{0m} but MM5 does not
180 distinguish them; (2) the two schemes apply different universal functions under stable condition; (3) Li considers the RSL
181 effect while MM5 ignores it.

182 3 Observational data and methods

183 The observational fluxes used in this study measured at Gucheng station from December 1, 2016 to January 9, 2017.
184 Gucheng station (115.40 E, 39.08 N) is located at Gucheng County, Baoding, Hebei province and it is about 110km
185 southwest of Beijing (Fig. 1a). This station has a farmland site where rice is planted in summer and wheat in winter. The
186 surroundings are mainly farmland and scattered villages (Fig. 1b). At Gucheng station, the momentum and sensible heat
187 fluxes near surface were measured by the eddy correlation flux measurement system. The system is mainly composed of a
188 sonic anemometer (CSAT3) and a gas analyzer (LI-7500). They are set up at 4m height above surface ground. The measured
189 fluxes are used to evaluate the two schemes as well as estimate the roughness lengths. The measured meteorological
190 variables including wind speed and direction, temperature, humidity, pressure, radiation are used to calculate the momentum
191 and sensible heat fluxes both in the Li and MM5 schemes. Note the observed meteorological data were from Gucheng station
192 and national basic automatic weather stations in Jing-Jin-Ji in east China, respectively. Hourly surface PM_{2.5} mass
193 concentration in Baoding and Beijing from China National Environmental Monitoring Centre (<http://www.cnemc.cn/>) were
194 also used in this paper.

195 3.1 Data processing

196 To obtain accurate flux data, quality control has been performed for the observational data, including: (1) eliminate the
197 outliers and the data in rainy days; (2) double rotation and WPL correction (Webb et al., 1980); (3) omit the dataset when the
198 wind speed is less than 0.5m/s. In addition, the wind field especially the wind direction has a great impact on the value of
199 z_{0m} , so it is necessary to understand the situation at Gucheng station. Fig. 2 shows the distribution frequency of wind speed
200 and wind direction at Gucheng during the observation (December 1, 2016 ~ January 9, 2017). The wind speed is stable
201 during this period and the maximum is no more than 5 m/s and most of them are about 1 ~ 2 m/s. The wind direction is
202 relatively uniform except for the southeast wind (135°).

203 3.2 Determination of surface skin temperature

204 The surface skin temperature at Gucheng station is calculated from the radiation data by the following formula:

$$205 R_{lw}^{\uparrow} = (1 - \varepsilon_s)R_{lw}^{\downarrow} + \varepsilon_s \sigma T_g^4, \quad (19)$$

206 where R_{lw}^{\uparrow} and R_{lw}^{\downarrow} are the surface upward longwave radiation and long wave radiation incident on the surface,
 207 respectively. σ is the Stephen Boltzmann constant, $\sigma = 5.67 \times 10^{-8} \text{Wm}^{-2}\text{K}^{-4}$. T_g is the surface skin temperature, ε_s is
 208 the surface emissivity which is the prerequisite for calculating T_g . Many researches estimated ε_s and the range of the values
 209 is always 0.9 ~ 1 (Stewart et al., 1994; Verhoef et al., 1997). According to the semi-empirical method in Yang et al. (2008),
 210 ε_s is estimated when the RMSE is minimal. In this paper, the Li and MM5 schemes were used to estimate the ε_s value (as
 211 shown in Fig. 3). It is clear that the ε_s value corresponding to the minimum RMSE is not very sensitive to the choice of two
 212 schemes. When ε_s is 1, the RMSE has the minimum value. Thus, this experiment takes 1 as the optimal value of ε_s .

213 3.3 Determination of roughness length z_{0m} (z_{0h})

214 Using the observed momentum and sensible heat fluxes and the meteorological variables including wind speed,
 215 temperature, humidity and pressure after quality control at Gucheng station, z_{0m} and z_{0h} were derived by Eqs. (20a) and
 216 (20b) following Yang et al. (2003) and Sicart et al. (2014).

$$217 \quad \frac{u_*}{u} = \frac{k}{\ln \frac{z}{z_{0m}} - \psi_M}, \quad (20a)$$

$$218 \quad \frac{\theta_*}{(\theta - \theta_g)} = \frac{k}{R[\ln \frac{z}{z_{0h}} - \psi_H]}. \quad (20b)$$

219 During the observation period, the crops stopped growing and the height did not exceed 0.1 m, so the zero-plane
 220 displacement height was ignored hence the reference height z was taken as 4m. The observation time was too short (about 1
 221 month) to consider the effect of seasonal variations on roughness lengths. Thus, z_{0m} and z_{0h} were assumed as two fixed
 222 values. Based on the variables and formulae mentioned above, the roughness lengths at Gucheng are derived: $z_{0m} =$
 223 0.0419 m, $z_{0h} = 0.0042$ m.

224 4 Results and discussion

225 The RSL, roughness length and their influence on the calculation of turbulent flux are discussed in detail in this section.
 226 The Li and MM5 schemes are offline tested and evaluated during the haze pollution from December 13 to 23, 2016.

227 4.1 The influence of RSL and roughness length on the calculation of turbulent flux

228 The RSL is usually defined as the region where the flow is influenced by the individual roughness elements as reflected
 229 by the spatial inhomogeneity of the mean flow (Florens et al., 2013). In the RSL, turbulence is strongly affected by
 230 individual roughness elements, and the standard MOST is no longer valid (Simpson et al., 1998). Therefore, it is necessary to
 231 consider the RSL effect in the calculation of turbulent fluxes, especially for the rough terrain such as forest or large cities.
 232 z_{0m} is defined as the height at which the extrapolated wind speed following the similarity theory vanishes. It is mainly
 233 determined by land-cover type and canopy height after excluding large obstructions. In models, z_{0m} is always based on the

234 look-up table which is related to land-cover types. In this study, z_{0m} was simply classified based on the research of Stull
 235 (1988) listed in Table 1. It can be seen in Table 1 that the rougher underlying surface corresponds to the larger value of z_{0m} .
 236 z_{0h} is the height at which the extrapolated air temperature is identical to the surface skin temperature. Some early researches
 237 assumed that z_{0m} was equal to z_{0h} (Louis, 1979; Louis et al., 1982). However, the assumption is not applicable in reality
 238 because z_{0m} and z_{0h} have different physical meanings. Different treatment of z_{0m} and z_{0h} may introduce considerable
 239 changes in the surface flux calculation (Launiainen, 1995; Kot and Song, 1998; Anurose and Subrahmanyam, 2013). Many
 240 studies removed the assumption that z_{0m} was equal to z_{0h} and made the schemes more applicable in the situation that z_{0m}
 241 was not equal to z_{0h} or the ratio of z_{0m} to z_{0h} was much large (Wouters et al., 2012; Li et al., 2014; Li et al., 2015).
 242 Some field experiments even indicated the ratio z_{0m}/z_{0h} has a diurnal variation (Sun, 1999; Yang, 2003; Yang, 2008). In
 243 this study, we make the common assumption that the ratio z_{0m}/z_{0h} is a constant.

244 Considering the lowest level in mesoscale models is usually about 10m, $z = 10$ m is set as the reference height. The
 245 range of Ri_B is set according to Louis82 (Louis et al., 1982) in the following discussion. Firstly, the effects of different
 246 land-cover types (different z_{0m} values) and RSL on flux calculation were discussed. Set $z_{0m} = z_{0h}$, corresponding to four
 247 cases: $z_{0m} = 1, 0.5, 0.05, 0.001$ m. These cases correspond to large cities, forests, agricultural fields and wide water surface,
 248 respectively. Fig. 4 shows the relationship between $C_M(C_H)$ and Ri_B for different z_{0m} values and treatment of RSL. It can
 249 be seen that both RSL and z_{0m} have impacts on C_M and C_H . Ignoring the RSL effect results in larger C_M and C_H ,
 250 compared with the results of original scheme considering the RSL. The difference induced by RSL is obvious only under the
 251 rough surface. For example, the difference under $z_{0m} = 1$ is obviously greater than other z_{0m} settings, and when z_{0m} is
 252 reduced to 0.05 or less, the RSL has little effect. Furthermore, the RSL contributes more to sensible heat transfer than to
 253 momentum transfer under the same setting of z_{0m} . The effects of different land-cover types on C_M and C_H are much more
 254 significant compared with RSL. The rougher the surface is (corresponding to the larger z_{0m} value), the larger the C_M (C_H)
 255 is. In addition, there is a corresponding relationship between $C_M(C_H)$ and stability. The more unstable the atmosphere is, the
 256 larger difference the value of $C_M(C_H)$ is and vice versa. Once Ri_B exceeds the critical value (generally 0.2~0.25), the
 257 transfer coefficients decline sharply but still above 0.

258 Secondly, the effects of difference between z_{0m} and z_{0h} as well as RSL on flux calculation are discussed. The
 259 relationship between z_{0m} and z_{0h} can be expressed as $kB^{-1} = \ln \frac{z_{0m}}{z_{0h}}$. Over the sea, z_{0m} is comparable to z_{0h} ; over the
 260 uniform vegetation surface (grassland, farmland, woodland), kB^{-1} is about 2 ($z_{0m}/z_{0h} \approx 10$) (Garratt and Hicks, 1973;
 261 Garratt, 1978; Garratt and Francey, 1978), which coincides with our results in Gucheng ($z_{0m} = 0.0419$ m, $z_{0h} =$
 262 0.0042 m); over the surface with bluff roughness elements, the kB^{-1} value may be very large. For example, in some large
 263 cities, kB^{-1} is even up to 30 ($z_{0m}/z_{0h} \approx 10^{13}$) (Sugawara and Narita, 2009). Therefore, the ratio z_{0m}/z_{0h} varies over a
 264 wide range. Fig. 5 shows the relationship between $C_M(C_H)$ and Ri_B for different treatment of z_{0m}/z_{0h} . Set $z_{0m} = 1$ as a

265 large city case, $z_{0h}=1, 0.01, 10^{-4}, 10^{-6}$ m, and the large differences derived from the different ratios are displayed in Fig. 5.
266 The similar RSL effect can be found compared with Fig. 4. The differences induced by RSL are more obvious than that in
267 Fig. 4. The different treatment of ratio z_{0m}/z_{0h} has great impact on turbulent flux transfer, particularly for sensible heat
268 transfer. It seems evident that when z_{0h} is not equal to z_{0m} ($z_{0m}/z_{0h}=100 \sim 10^6$), the calculated C_H is much small
269 compared to the treatment that z_{0h} is equal to z_{0m} ($z_{0m}/z_{0h}=1$). In addition, $C_M(C_H)$ decreases with the increase of
270 stability, and they decrease much slower when z_{0h} is not equal to z_{0m} .

271

272 4.2 Comparison of momentum and sensible heat fluxes calculated by the two schemes

273 Using the obtained roughness lengths and the observations, the momentum and sensible heat flux were calculated by the
274 Li and MM5 schemes. Firstly, z_{0m} and z_{0h} were set as 0.0419 and 0.0042 respectively in the Li scheme, z_0 was equal to
275 z_{0m} in the MM5 scheme to calculate the momentum and sensible heat fluxes and the results are shown in Figs. 6a and 6b. It
276 can be seen that compared with MM5, Li performs better with higher regression coefficient and determination coefficient.
277 For the momentum fluxes, the regression coefficient by Li is 0.6795 and that by MM5 is 0.5598, indicating that the error of
278 Li is 12% lower than that of MM5. For sensible heat fluxes, the regression coefficient by Li is 0.7967 and that by MM5 is
279 1.7994. The latter is much larger than 1, that is, the MM5 scheme obviously overestimates the sensible heat due to it does not
280 distinguish z_{0h} from z_{0m} . Then, make z_0 equal to 0.0042 in the MM5 scheme to re-calculate the sensible heat fluxes as
281 shown in Fig. 6c. It can be seen the result has a great improvement after modifying z_0 value and the regression coefficient
282 by MM5 is 0.7363, indicating that the error was reduced by 54% after considering the z_{0h} effect. The result indicates that
283 z_{0h} plays a key role in both the SL scheme and the sensible heat flux (Chen and Zhang, 2009; Chen et al., 2011). However,
284 the error caused by Li is still 6% lower than that by MM5. This illustrates that in addition to the effect of roughness lengths,
285 the algorithm of the Li scheme itself is more reasonable than that of MM5 scheme.

286 4.3 The specific performance of the two schemes in the severe haze pollution

287 There were two obvious pollution processes during this observation period and one occurred during December 13 to 23,
288 2016. Fig. 7 shows the variations of hourly observed $PM_{2.5}$ concentration as well as the momentum and sensible heat fluxes
289 calculated by the Li and MM5 schemes at Gucheng station in this process. For the research purpose significance, only the
290 daytime (from 8:00 a.m. to 20:00 p.m.) was taken into account. Note in MM5, z_0 was 0.0419 when calculate momentum
291 fluxes and it was 0.0042 when calculate sensible heat fluxes. As shown in Fig. 7, the calculated results of momentum and
292 sensible heat fluxes for the two schemes are generally consistent with the trend of the observations. Specifically, for the
293 momentum fluxes (Fig. 7a), the results of two schemes have little difference when the values of observed momentum fluxes
294 are large or at the peak. When the observed momentum fluxes are small, the Li scheme results are close to or less than the

295 observations, while the MM5 scheme results are always higher than observations because of the limit of $u_* = 0.1$ in this
296 scheme. For the sensible heat fluxes (Fig. 7b), MM5 results are always lower while Li results are closer to observations
297 especially when the observed values are small. Furthermore, according to the evolution of $PM_{2.5}$ concentration, this haze
298 event was then divided into three stages: the clear stage (stage 1: 13~14), the transition stage (stage 2: 16~18) and the
299 maintenance stage (stage 3: 21~22). As shown in Fig. 7, in the clear stage (stage 1), the atmospheric stratification is unstable,
300 $PM_{2.5}$ concentration is low and there is a strong flux transport in the SL, the corresponding observations of the momentum
301 and sensible heat fluxes are relatively high and they vary greatly. In the transition stage (stage 2), the atmosphere is changing
302 from unstable to stable corresponding to hazes formation, the momentum and sensible heat fluxes gradually decreases and
303 the daily variation also decreases. In the maintenance stage (stage 3), the atmospheric stratification is very stable, and flux
304 transport in the SL is weak, both the momentum and sensible heat fluxes are at a low level. It can be seen that the Li results
305 are generally closer to the observations compared with MM5 results in all three stages.

306 Fig. 8 shows the probability distribution functions (PDF) of the difference of momentum fluxes (Figs. 8a, 8c, 8e, 8g)
307 and sensible heat fluxes (Figs. 8b, 8d, 8f, 8h) calculated by using the Li and MM5 schemes in different stages at Gucheng
308 station. In the whole pollution process, for the momentum fluxes (Fig. 8a), the PDF of the difference by Li tends to cluster in
309 a narrower range centered by 0, and the probability within $\pm 0.005N\ m^{-2}$ is 46.82%, while this value by MM5 falls to 23.02%.
310 For the sensible heat fluxes (Fig. 8b), the PDF of the difference by Li is also more concentrated around 0 than that by MM5.
311 The probabilities of bias by Li and MM5 within $\pm 2.5W\ m^{-2}$ are 32.54% and 13.49%, respectively. In stage 1, for the
312 momentum fluxes (Fig. 8c), the probability of bias by Li within $\pm 0.005N\ m^{-2}$ is 38.09%. The bias of MM5 mainly
313 concentrates larger than 0, and the probability within $\pm 0.005N\ m^{-2}$ is 14.29%. For the sensible heat fluxes (Fig. 8d), the
314 probability of Li bias within $\pm 2.5W\ m^{-2}$ is 38.09%, the same as momentum fluxes. The bias of MM5 mainly concentrates
315 less than 0, and the probability within $\pm 2.5W\ m^{-2}$ is 9.52%. In stage 2, the differences between the two schemes are more
316 obvious. The momentum and sensible heat fluxes bias by Li is the most concentrated around 0 in all cases, while the
317 distribution of bias by MM5 is similar to that in stage 1. Specifically, for the momentum fluxes (Fig. 8e), the probabilities of
318 bias by Li and MM5 within $\pm 0.005N\ m^{-2}$ are 56.25% and 25.00%. For the sensible heat fluxes (Fig. 8f), the probabilities of
319 bias by Li and MM5 within $\pm 2.5W\ m^{-2}$ are 40.62% and 6.25%. In stage 3, the difference between two schemes is small. For
320 the momentum fluxes (Fig. 8g), the probabilities of bias by Li and MM5 within $\pm 0.005N\ m^{-2}$ are 22.73% and 27.27%. For
321 the sensible heat fluxes (Fig. 8h), the probabilities of bias by Li and MM5 within $\pm 2.5W\ m^{-2}$ are both 36.36%.

322 Mean bias (MB), normalized mean bias (NMB), normalized mean error (NME) and root mean square error (RMES) of
323 Li and MM5 were calculated to test the two schemes. Table 2 shows that the Li scheme generally estimates better than the
324 MM5 scheme. In the whole haze process, the Li scheme underestimates the momentum fluxes by 3.63% relative to the
325 observations, while the MM5 scheme overestimates by 34.03%. The Li and MM5 schemes underestimate the sensible heat

326 fluxes by 15.69% and 50.22%, respectively. In the three stages, the Li scheme performs much better than the MM5 scheme
 327 in the stage 1 and stage 2, especially in stage 2 when atmospheric stratification transforms from unstable to stable condition,
 328 the difference between the Li and MM5 schemes are particularly significant. The Li and MM5 schemes overestimate the
 329 momentum fluxes by 7.68% and 45.56%, respectively, while Li and MM5 underestimate the sensible heat fluxes by 33.84%
 330 and 76.88%. The error of Li is much less than that of MM5. Considering the importance of atmospheric stratification in the
 331 generation and accumulation of $PM_{2.5}$ in stage 2, the Li scheme is expected to show better performance in online simulation
 332 of $PM_{2.5}$ than MM5.

333 Based on the good behavior of the Li scheme in Gucheng, the same experiment was performed at Beijing station to
 334 discuss the effect of different land-cover types on flux calculation for two schemes. For Beijing station, the assumption
 335 $z_{0m} = 1m$, $z_{0m}/z_{0h} = 10^6$ was made to represent the surface condition of megacity due to a lack in situ measurements of
 336 surface turbulent flux. As shown in Fig. 9, the evolution of $PM_{2.5}$ concentration at Beijing station was also divided into three
 337 stages (stage 1: 13~15; stage 2: 17~19; stage 3: 20~21) just like Gucheng in the discussion. Compare to Fig. 7, there is a
 338 significant increase in the difference of momentum and sensible heat fluxes between Li and MM5 in Fig. 9. To be specific,
 339 the momentum transfer in Beijing is obviously larger than that in Gucheng due to the great increase of the urban
 340 aerodynamic roughness length (z_{0m}). In the meanwhile, the difference between Li and MM5 has a further expansion at
 341 Beijing station compared with Gucheng. The sensible heat transfer by the Li scheme has great difference between clear days
 342 and pollution days, which is, the sensible heat transfer changes acutely in the stage 1 while it changes smoothly in the stage 2
 343 and stage 3. The sensible heat transfer by the MM5 scheme is significantly different compared with Li result due to MM5
 344 ignored the z_{0m} effect, and the small number of z_{0h} keeps the sensible heat fluxes at a low level in all three stages.

345 To quantify the differences between the two schemes, a relative difference is defined in percentage:

$$346 \quad \Delta V = \left| \frac{V_{Li} - V_{MM5}}{V_{MM5}} \right| \times 100\%, \quad (21)$$

347 where V_{Li} and V_{MM5} are the momentum (or sensible heat) flux calculated by the Li and MM5 schemes, respectively. We
 348 obtained the relative differences at the two stations in the three stages through the statistics. It is clearly that the largest
 349 relative difference at Gucheng station is in the stage 2 and the value at Beijing station is in the stage 1. The differences in
 350 Beijing are always larger than that in Gucheng for each three stages. Specifically, the relative difference of momentum flux
 351 in stage 1, stage 2 and stage 3 increases by 73%, 34% and 27%, respectively, and the results of sensible heat flux are 289%,
 352 52% and 68%, respectively.

353 We further tested the two schemes in whole Jing-Jin-Ji region. Fig. 10 shows the mean momentum and sensible heat
 354 fluxes calculated by Li and MM5 schemes and their difference in Jing-Jin-Ji during the pollution episode. The assumption
 355 $z_{0m} = 0.1m$, $z_{0m}/z_{0h} = 10^3$ were used to represent the average condition of the underlying surface of Jing-Jin-Ji region.
 356 As shown in Fig. 10, the momentum fluxes calculated by Li are less than that by MM5 in most stations; the sensible heat

357 fluxes calculated by Li are usually larger than that by MM5. The result is consistent with the experiment of Gucheng station,
358 which further indicates the importance of considering z_{0m} and z_{0h} at the same time.

359 5 Conclusions

360 Using the observed momentum and sensible heat fluxes, together with conventional meteorological data including
361 pressure, temperature, humidity and wind speed from December 1, 2016 to January 9, 2017, including a severe pollution
362 episode from December 13 to 23, 2016, the differences and the performance of the two surface schemes were discussed and
363 evaluated in this paper. The evolution process of atmospheric stratification from unstable to stable corresponding to $PM_{2.5}$
364 increasing was mainly discussed. The contributions of roughness lengths (z_{0m} and z_{0h}) and other factors in the SL schemes
365 to the momentum and sensible heat flux calculation were also discussed in details. The results are summarized as follows:

366 1) z_{0m} and z_{0h} have important effects on turbulent flux calculation in the SL schemes. Different values of z_{0m} and
367 z_{0h} in the schemes could induce great changes in flux calculation, indicating that it is very necessary and important to
368 distinguish z_{0h} from z_{0m} . Ignoring the difference between the two in the MM5 scheme led to large errors in calculation of
369 sensible heat fluxes and this error in Gucheng is 54%. Besides the roughness lengths, the algorithms of two schemes are also
370 one of important factors. In addition, ignoring the effect of the RSL in schemes may also results in certain bias of momentum
371 and sensible heat fluxes in megacity regions which represent the rough underlying surface.

372 2) The effect of z_{0m}/z_{0h} on turbulent fluxes is closely related to the land-cover types (z_{0m}). A rough land-cover type
373 (large z_{0m}) should be accompanied by a large value of z_{0m}/z_{0h} . The differences of momentum and sensible heat fluxes
374 calculated by Li and MM5 were much bigger in Beijing than that in Gucheng. This suggests that the MM5 scheme probably
375 induces bigger error in megacities with rough surface (e.g., Beijing) than it in suburban area with smooth surface (e.g.,
376 Gucheng) due to the irrational algorithm of MM5 scheme itself and the ignoring difference between z_{0m} and z_{0h} .

377 3) The Li scheme generally performed better than the MM5 scheme in the calculation of both the momentum flux and
378 the sensible heat flux compared with observations at Gucheng station. The Li scheme made a better description in
379 atmospheric stratification which is closely related to the haze pollution, compared with the MM5 scheme. This advantage
380 was the most prominent in the transition stage from unstable to stable atmospheric stratification corresponding to the $PM_{2.5}$
381 accumulation. In this stage, the momentum flux calculated by Li was overestimated by 7.68% and this overestimation by
382 MM5 was up to 45.56%; the sensible heat flux by Li was underestimated by 33.84% while this underestimation by MM5
383 was even up to 76.88%. In most Jing-Jin-Ji region, the momentum fluxes calculated by Li were less than that by MM5 and
384 the sensible heat fluxes by Li were larger than that by MM5, which was consistent with Gucheng.

385 The offline study of the two SL schemes in this paper showed the superiority of the Li scheme for surface flux
386 calculation corresponding to the $PM_{2.5}$ evolution during the haze episode in Jing-Jin-Ji in east China. The study results offer

387 the prerequisite and a possible way to improve PBL diffusion simulation and then PM_{2.5} prediction, which will be achieved
388 in the follow-up work of online integrating of the Li scheme into the atmosphere chemical model.

389 **Acknowledgments**

390 The study was supported by the National Key Project (2016YFC0203306), the National (Key) Basic Research and
391 Development (973) Program of China (2014CB441201), the National Key Project (2016YFC0203304)

392 **References**

- 393 Anurose, T. J., and Subrahmanyam, D. B.: Improvements in Sensible Heat-Flux Parametrization in the High-Resolution
394 Regional Model (HRM) Through the Modified Treatment of the Roughness Length for Heat, Bound.-Lay. Meteorol.,
395 147, 569-578, <https://doi.org/10.1007/s10546-013-9799-9>, 2013.
- 396 Ban, J., Gao, Z., and Lenschow, D. H.: Climate simulations with a new air-sea turbulent flux parameterization in the
397 National Center for Atmospheric Research Community Atmosphere Model (CAM3), J. Geophys. Res.-Atmos., 115,
398 <https://doi.org/10.1029/2009JD012802>, 2010.
- 399 Beljaars, A. C. M., and Holtslag, A. A. M.: Flux parameterization over land surfaces for atmospheric models, J. Appl.
400 Meteor., 30, 327-341, 1991.
- 401 Businger, J. A., Wyngaard, J. C., Izumi, Y., and Bradley, E. F.: Flux-profile relationships in the atmospheric surface layer, J.
402 Atmos. Sci., 28, 181-189, 1971.
- 403 Businger, J. A.: Transfer of momentum and heat in the planetary boundary layer, Proc. Symp. Arctic Heat Budget and
404 Atmospheric Circulation, RM-5233-NSF, 305-331, 1966.
- 405 Chen, F., and Zhang, Y.: On the coupling strength between the land surface and the atmosphere: From viewpoint of surface
406 exchange coefficients, Geophys. Res. Lett., 36, <https://doi.org/10.1029/2009GL037980>, 2009.
- 407 Chen, Y., Yang, K., He, J., Qin, J., Shi, J., Du, J., and He, Q.: Improving land surface temperature modeling for dry land of
408 China, J. Geophys. Res.-Atmos., 116, <https://doi.org/10.1029/2011JD015921>, 2011.
- 409 Cheng, F. Y., Chin, S. C., and Liu, T. H.: The role of boundary layer schemes in meteorological and air quality simulations of
410 the Taiwan area, Atmos. Environ., 54, 714-727, <https://doi.org/10.1016/j.atmosenv.2012.01.029>, 2012.
- 411 Cheng, Y., and Brutsaert, W.: Flux-profile relationships for wind speed and temperature in the stable atmospheric boundary
412 layer, Bound.-Lay. Meteorol., 114, 519-538, <https://doi.org/10.1007/s10546-004-1425-4>, 2005.
- 413 De Ridder, K.: Bulk Transfer Relations for the Roughness Sublayer, Bound.-Lay. Meteorol., 134, 257-267,
414 <https://doi.org/10.1007/s10546-009-9450-y>, 2010.

415 Dyer, A. J.: A review of flux-profile relationships, *Bound.-Lay. Meteorol.*, 7, 363-372, <https://doi.org/10.1007/BF00240838>,
416 1974.

417 Dyer, A. J.: The turbulent transport of heat and water vapour in an unstable atmosphere, *Quart. J. Roy. Meteor. Soc.*, 93,
418 501-508, <https://doi.org/10.1002/qj.49709339809>, 1967.

419 Florens, E., Eiff, O., and Moulin, F.: Defining the roughness sublayer and its turbulence statistics, *Exp. Fluids*, 54, 1500,
420 <https://doi.org/10.1007/s00348-013-1500-z>, 2013.

421 Garratt, J. R., and Francey, R. J.: Bulk characteristics of heat transfer in the unstable, baroclinic atmospheric boundary layer,
422 *Bound.-Lay. Meteorol.*, 15, 399-421, <https://doi.org/10.1007/BF00120603>, 1978.

423 Garratt, J. R., and Hicks, B. B.: Momentum, heat and water vapour transfer to and from natural and artificial surfaces, *Quart.*
424 *J. Roy. Meteor. Soc.*, 99, 680-687, 1973.

425 Garratt, J. R.: Transfer characteristics for a heterogeneous surface of large aerodynamic roughness, *Quart. J. Roy. Meteor.*
426 *Soc.*, 104, 491-502, 1978.

427 Högström, U.: Review of some basic characteristics of the atmospheric surface layer, *Bound.-Lay. Meteorol.*, 78, 215-246,
428 <https://doi.org/10.1007/BF00120937>, 1996.

429 Holtslag, A. A. M., and De Bruin, H. A. R.: Applied modeling of the nighttime surface energy balance over land, *J. Appl.*
430 *Meteor.*, 27, 689-704, 1988.

431 Hu, X. M., Nielsen-Gammon, J. W., and Zhang, F.: Evaluation of three planetary boundary layer schemes in the WRF model,
432 *J. Appl. Meteorol. Climatol.*, 49, 1831-1844, <https://doi.org/10.1175/2010JAMC2432.1>, 2010.

433 Jiménez, P. A., Dudhia, J., González-Rouco, J. F., Navarro, J., Montávez, J. P., and García-Bustamante, E.: A revised scheme
434 for the WRF surface layer formulation, *Mon. Wea. Rev.*, 140, 898-918, <https://doi.org/10.1175/MWR-D-11-00056.1>,
435 2012.

436 Kot, S. C., and Song, Y.: An Improvement of the Louis Scheme for the Surface Layer in an Atmospheric Modelling System,
437 *Bound.-Lay. Meteorol.*, 88, 239-254, <https://doi.org/10.1023/A:1001119329423>, 1998.

438 Launiainen, J.: Derivation of the relationship between the Obukhov stability parameter and the bulk Richardson number for
439 flux-profile studie, *Bound.-Lay. Meteorol.*, 76, 165-179, <https://doi.org/10.1007/BF00710895>, 1995.

440 Li, T., Wang, H., Zhao, T., Xue, M., Wang, Y., Che, H., and Jiang, C.: The Impacts of Different PBL Schemes on the
441 Simulation of PM_{2.5} during Severe Haze Episodes in the Jing-Jin-Ji Region and Its Surroundings in China, *Adu.*
442 *Meteorol.*, <http://dx.doi.org/10.1155/2016/6295878>, 2016a.

443 Li, Y., Gao, Z., Li, D., Chen, F., Yang, Y., and Sun, L.: An Update of Non-iterative Solutions for Surface Fluxes Under
444 Unstable Conditions, *Bound.-lay. Meteorol.*, 156, 501-511, <https://doi.org/10.1007/s10546-015-0032-x>, 2015.

445 Li, Y., Gao, Z., Li, D., Chen, F., Yang, Y., and Sun, L.: Erratum to: An Update of Non-iterative Solutions for Surface Fluxes
446 Under Unstable Conditions, *Bound.-Lay. Meteorol.*, 161: 225-228, 2016b.

447 Li, Y., Gao, Z., Li, D., Wang, L., and Wang, H.: An improved non-iterative surface layer flux scheme for atmospheric stable
448 stratification conditions, *Geosci. Model Dev.*, 7, 515-529, <https://doi.org/10.5194/gmd-7-515-2014>, 2014.

449 Li, Y.: *On the Surface Turbulent Fluxes Calculation in Numerical Models*, Beijing: university of Chinese academy of
450 sciences, 2014.

451 Li, Z., Guo, J., Ding, A., Liao, H., Liu, J., Sun, Y., Wang, T., Xue, H., Zhang, H., and Zhu, B.: Aerosol and boundary-layer
452 interactions and impact on air quality, *Natl. Sci. Rev.*, 4, 810–833, <https://doi.org/10.1093/nsr/nwx117>, 2017.

453 Liu, T. T., Gong, S. L., He, J. J., Yu, M., Wang, Q. F., Li, H. R., Liu, W., Zhang, J., Li, L., Wang, X. G., Li, S. L., Lu, Y. L.,
454 Du, H. T., Wang, Y. Q., Zhou, C. H., Liu, H. L. and Zhao, Q. C.: Attributions of meteorological and emission factors to
455 the 2015 winter severe haze pollution episodes in China’s Jing-Jin-Ji area, *Atmos. Chem. Phys.*, 17, 2971–2980,
456 <https://doi.org/10.5194/acp-17-2971-2017>, 2017.

457 Louis, J. F.: A parametric model of vertical eddy fluxes in the atmosphere. *Bound.-Lay. Meteorol.*, 17, 187-202,
458 <https://doi.org/10.1007/BF00117978>, 1979.

459 Louis, J. F., Tiedtke, M., and Geleyn, J. F.: A short history of the operational PBL parameterization at ECMWF, in *Workshop*
460 *on Planetary Boundary Layer Parameterization*, November 1981, ECMWF, Reading, U.K., pp. 59–79, 1982.

461 Monin, A. S., and Obukhov, A. M.: Basic laws of turbulent mixing in the surface layer of the atmosphere, *Contrib. Geophys.*
462 *Inst. Acad. Sci., USSR*, 24, 163–187, 1954.

463 Paulson, C. A.: The mathematical representation of wind speed and temperature profiles in the unstable atmospheric surface
464 layer, *J. Appl. Meteorol.*, 9, 857-861, 1970.

465 Sharan, M., and Srivastava, P.: A Semi-Analytical Approach for Parametrization of the Obukhov Stability Parameter in the
466 Unstable Atmospheric Surface Layer, *Bound.-Lay. Meteorol.*, 153, 339-353, <https://doi.org/10.1007/s10546-014-9948-9>,
467 2014.

468 Sicart, J. E., Litt, M., Helgason, W., Tahar, V. B., and Chaperon, T.: A study of the atmospheric surface layer and roughness
469 lengths on the high-altitude tropical Zongo glacier, Bolivia, *J. Geophys. Res.-Atmos.*, 119, 3793–3808,
470 <https://doi.org/10.1002/2013JD020615>, 2014.

471 Simpson, I. J., Thurtell, G. W., Neumann, H. H., Den Hartog, G., and Edwards, G. C.: The Validity of Similarity Theory in
472 the Roughness Sublayer Above Forests, *Bound.-Lay. Meteorol.*, 87, 69-99, <https://doi.org/10.1023/A:1000809902980>,
473 1998.

474 Stewart, J. B., Kustas, W. P., Humes, K. S., Nichols, W. D., Moran, M. S., and De Bruin, H. A. R.: Sensible heat
475 flux-radiometric surface temperature relationship for eight semiarid areas, *J. Appl. Meteorol.*, 33, 1110-1117, 1994.

476 Stull, R. B.: *An Introduction to Boundary Layer Meteorology*, Kluwer Academic Publishers, London, 1988.

477 Sugawara, H., and Narita, K.: Roughness length for heat over an urban canopy, *Theor. Appl. Climatol.*, 95, 291-299,
478 <https://doi.org/10.1007/s00704-008-0007-7>, 2009.

479 Sun, J.: Diurnal Variations of Thermal Roughness Height over a Grassland, *Bound.-Lay. Meteorol.*, 92, 407-427,
480 <https://doi.org/10.1023/A:1002071421362>, 1999.

481 Tymvios, F., Charalambous, D., Michaelides, S., and Lelieveld, J.: Intercomparison of boundary layer parameterizations for
482 summer conditions in the eastern Mediterranean island of Cyprus using the WRF-ARW model, *Atmos. Res.*, 208, 45-59,
483 <https://doi.org/10.1016/j.atmosres.2017.09.011>, 2017.

484 Vautard, R., Moran, M. D., Solazzo, E., Gilliam, R. C., Matthias, V., Bianconi, R., Chemel, C., Ferreira, J., Geyer, B.,
485 Hansen, A. B., Jericevic, A., Prank, M., Segers, A., Silver, J. D., Werhahn, J., Eolke, R., Rao, S. T., and Galmarini, S.:
486 Evaluation of the meteorological forcing used for the Air Quality Model Evaluation International Initiative (AQMEII)
487 air quality simulations, *Atmos. Environ.*, 53, 15-37, <https://doi.org/10.1016/j.atmosenv.2011.10.065>, 2012.

488 Verhoef, A., De Bruin, H. A. R., and Van Den Hurk, B. J. J. M.: Some Practical Notes on the Parameter kB-1 for Sparse
489 Vegetation., *J. Appl. Meteorol.*, 36, 560-572, 1997.

490 Wang, H., Shi, G. Y., Zhang, X. Y., Gong, S. L., Tan, S. C., Chen, B., Che, H. Z., and Li, T.: Mesoscale modeling study of the
491 interactions between aerosols and PBL meteorology during a haze episode in China Jing-Jin-Ji and its near surrounding
492 region - Part 2: Aerosols' radiative feedback effects, *Atmos. Chem. Phys.*, 15, 3277-3287,
493 <https://doi.org/10.5194/acp-15-3277-2015>, 2015b.

494 Wang, H., Tan, S. C., Wang, Y., Jiang, C., Shi, G., Zhang, M., and Che, H. Z.: A multisource observation study of the severe
495 prolonged regional haze episode over eastern China in January 2013, *Atmos. Environ.*, 89, 807-815,
496 <https://doi.org/10.1016/j.atmosenv.2014.03.004>, 2014.

497 Wang, H., Xue, M., Zhang, X. Y., Liu, H. L., Zhou, C. H., Tan, S. C., Che, H. Z., Chen, B., and Li, T.: Mesoscale modeling
498 study of the interactions between aerosols and PBL meteorology during a haze episode in China Jing-Jin-Ji and its
499 nearby surrounding region - Part 1: Aerosol distributions and meteorological features, *Atmos. Chem. Phys.*, 15,
500 3257-3275, <https://doi.org/10.5194/acp-15-3257-2015>, 2015a.

501 Wang, S., Wang, Q., and Doyle, J.: Some improvements to Louis surface flux parameterization. Paper presented at 15th
502 symposium on boundary layers and turbulence, American Meteorological Society, 15-19, 2002, Wageningen,
503 Netherlands.

504 Webb, E. K., Pearman, G. I., and Leuning, R.: Correction of flux measurements for density effects due to heat and water
505 vapour transfer, *Quart. J. Roy. Meteor. Soc.*, 106, 85-100, 1980.

506 Webb, E. K.: Profile relationships: The log-linear range, and extension to strong stability, *Quart. J. Roy. Meteor. Soc.*, 96,
507 67-90, 1970.

508 Wouters, H., De Ridder, K., and van Lipzig, N. P. M.: Comprehensive Parametrization of Surface-Layer Transfer
509 Coefficients for Use in Atmospheric Numerical Models, *Bound.-Lay. Meteorol*, 145, 539-550,
510 <https://doi.org/10.1007/s10546-012-9744-3>, 2012.

511 Xie, B., Fung, J. C. H., Chan, A., and Lau, A.: Evaluation of nonlocal and local planetary boundary layer schemes in the
512 WRF model, *J. Geophys. Res.-Atmos.*, 117, 48-50, <https://doi.org/10.1029/2011JD017080>, 2012.

513 Yang, K., Koike, T., and Yang, D.: Surface Flux Parameterization in the Tibetan Plateau, *Bound.-Lay. Meteorol.*, 106,
514 245-262, <https://doi.org/10.1023/A:1021152407334>, 2003.

515 Yang, K., Koike, T., Ishikawa, H., Kim, J., Li, X., Liu, H., Liu, S., Ma, Y., and Wang, J.: Turbulent Flux Transfer over
516 Bare-Soil Surfaces: Characteristics and Parameterization, *J. Appl. Meteorol. Clim.*, 47, 276-290,
517 <https://doi.org/10.1175/2007jamc1547.1>, 2008.

518 Yang, K., Tamai, N., and Koike, T.: Analytical Solution of Surface Layer Similarity Equations, *J. Appl. Meteorol.*, 40,
519 1647-1653, 2001.

520 Yang, Y., Liu, X., Qu, Y., Wang, J., An, J., Zhang, Y., and Zhang, F.: Formation mechanism of continuous extreme haze
521 episodes in the megacity Beijing, China, in January 2013, *Atmos. Res.*, 155, 192–203,
522 <https://doi.org/10.1016/j.atmosres.2014.11.023>, 2015.

523 Zhang, B., Wang, Y., and Hao, J.: Simulating aerosol-radiationcloud feedbacks on meteorology and air quality over eastern
524 China under severe haze conditions in winter, *Atmos. Chem. Phys.*, 15, 2387–2404,
525 <http://doi.org/10.5194/acp-15-2387-2015>, 2015.

526 Zhang, D., and Anthes, R. A.: A high-resolution model of the planetary boundary layer—Sensitivity tests and comparisons
527 with SESAME-79 data, *J. Appl. Meteorol.*, 21, 1594-1609, 1982.

528 Zhang, R., Li, Q., and Zhang, R.: Meteorological conditions for the persistent severe fog and haze event over eastern China
529 in January 2013, *Sci. China Earth Sci.*, 57, 26–35, <https://doi.org/10.1007/s11430-013-4774-3>, 2014.

530 Zhong, J., Zhang, X., Dong, Y., Wang, Y., Liu, C., Wang, J., Zhang, Y., and Che, H.: Feedback effects of boundary-layer
531 meteorological factors on cumulative explosive growth of PM_{2.5} during winter heavy pollution episodes in Beijing
532 from 2013 to 2016, *Atmos. Chem. Phys.*, 18, 247–258, <https://doi.org/10.5194/acp-18-247-2018>, 2018.

533

534 **Table 1.** Typical values of z_{0m} corresponding to various land-cover types

z_{0m}/m	Land-cover types
5~50	Mountain (above 100m)
1~5	The center of large cities, hills or mountain area
0.1~1	Forests, the center of large towns
0.01~0.1	Flat grasslands, agricultural fields
10^{-4} ~ 10^{-3}	The snow surface, wide water surface, flat deserts
10^{-5}	The ice surface

535

536

537

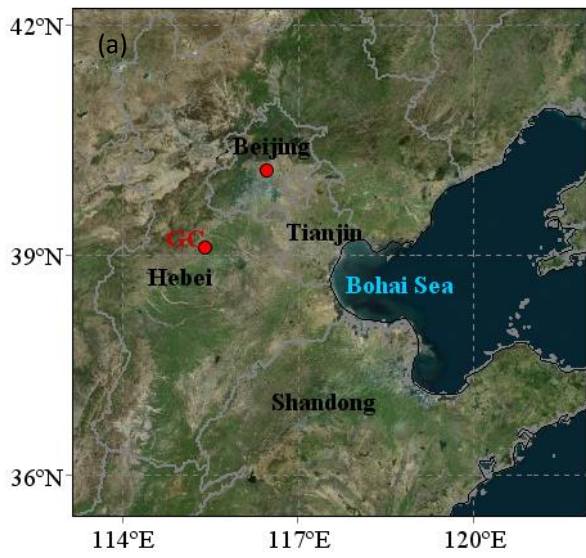
538 **Table 2.** Statistics between the Li and MM5 schemes calculated turbulent flux at Gucheng station.

		Li				MM5			
		MB	NMB	NME	RMSE	MB	NMB	NME	RMSE
Whole	τ	-0.0006	-3.63%	54.29%	0.0142	0.0058	34.03%	63.59%	0.0143
process	H	-2.2723	-15.69%	52.73%	10.9649	-7.2735	-50.22%	69.68%	12.7946
Stage 1	τ	0.0021	9.98%	55.90%	0.0172	0.0091	43.45%	66.66%	0.0169
	H	1.1775	5.79%	37.87%	10.5734	-7.1891	-35.34%	55.70%	13.1324
Stage 2	τ	0.0013	7.68%	44.50%	0.0111	0.0079	45.56%	56.81%	0.0121
	H	-4.5752	-33.84%	50.28%	9.3995	-10.3924	-76.88%	81.40%	13.2553
Stage 3	τ	-0.0024	-13.25%	59.13%	0.0144	0.0030	16.72%	56.34%	0.0138
	H	1.2818	11.39%	66.31%	11.4778	-1.7479	-15.52%	65.90%	10.4219

539 * τ : momentum flux; H: sensible heat flux; MB: mean bias; NMB: normalized mean bias; NME: normalized mean error;

540 RMSE: root mean square error. The units of MB and RMSE: $\mu\text{g} \cdot \text{m}^{-3}$.

541



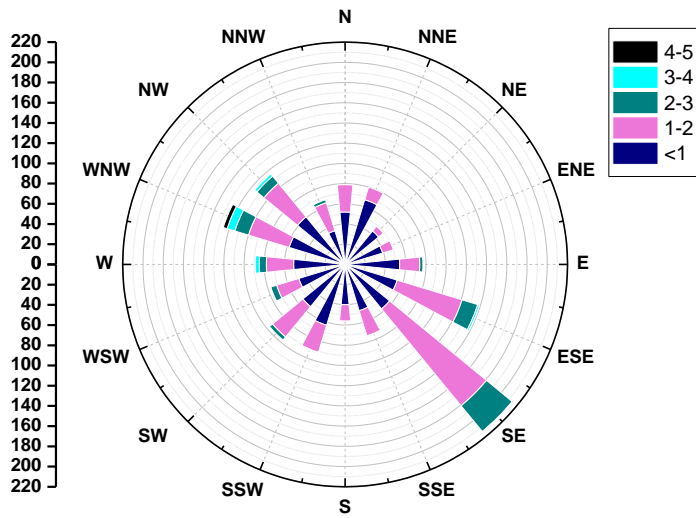
542

543 **Figure 1.** Location (a) and geographical environment (b) at Gucheng station. The map is from Bing Maps.

544

545

546



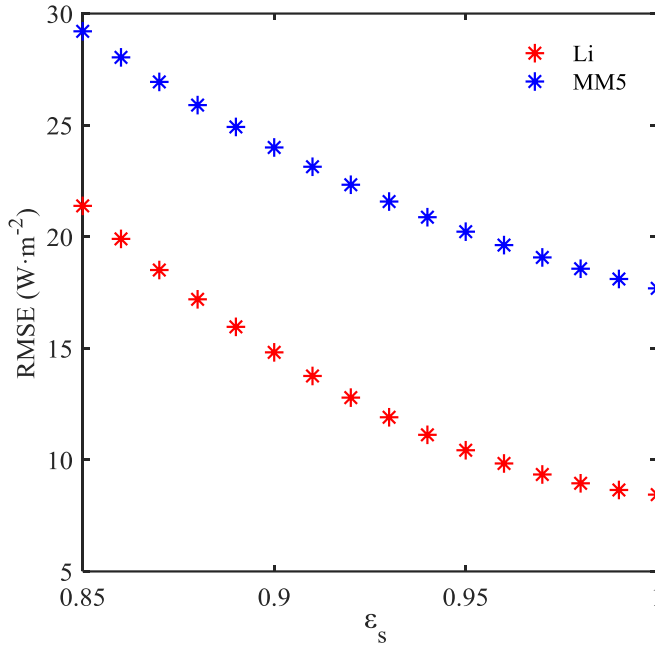
547

548 **Figure 2.** Wind Rose map at Gucheng station from December 1, 2016 to January 9, 2017.

549

550

551



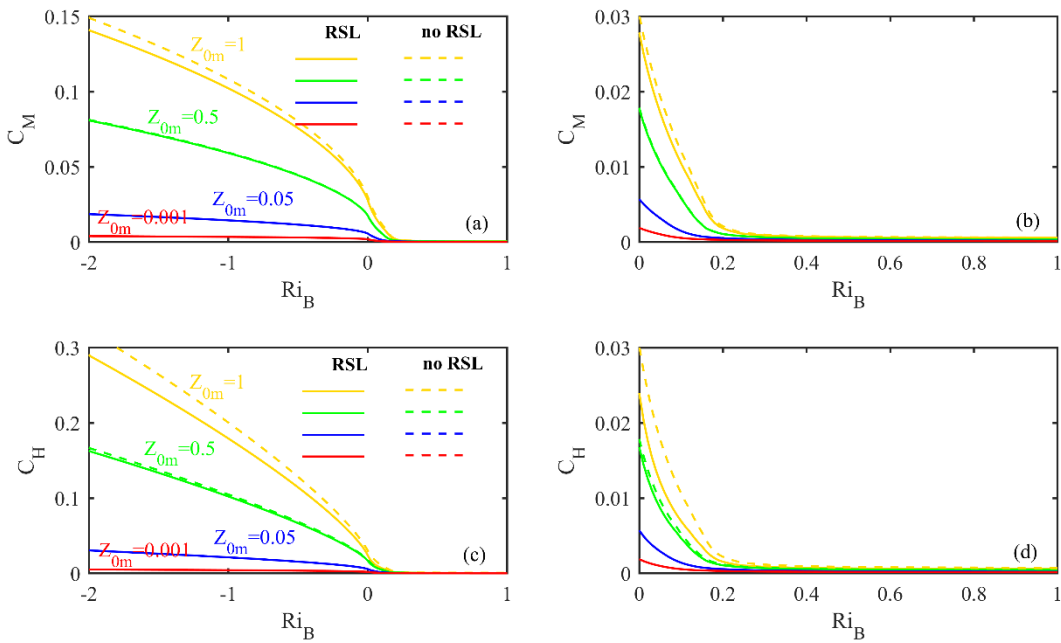
552

553 **Figure 3.** The surface emissivity ε_s dependence of RMSE between observed near-neutral heat fluxes and parameterized
 554 heat fluxes (red for Li and blue for MM5) at Gucheng station.

555

556

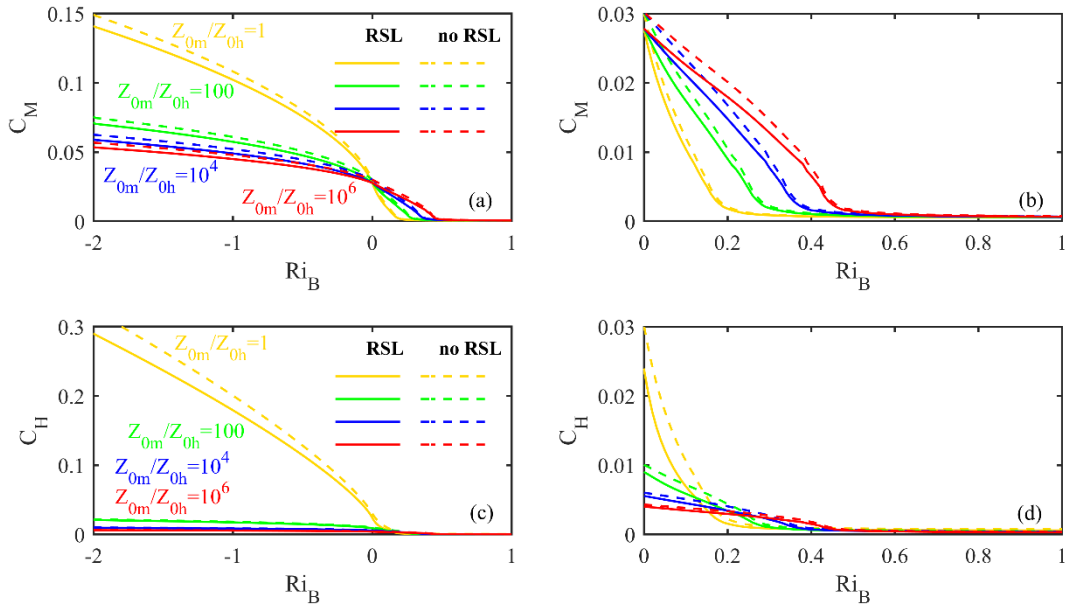
557



558

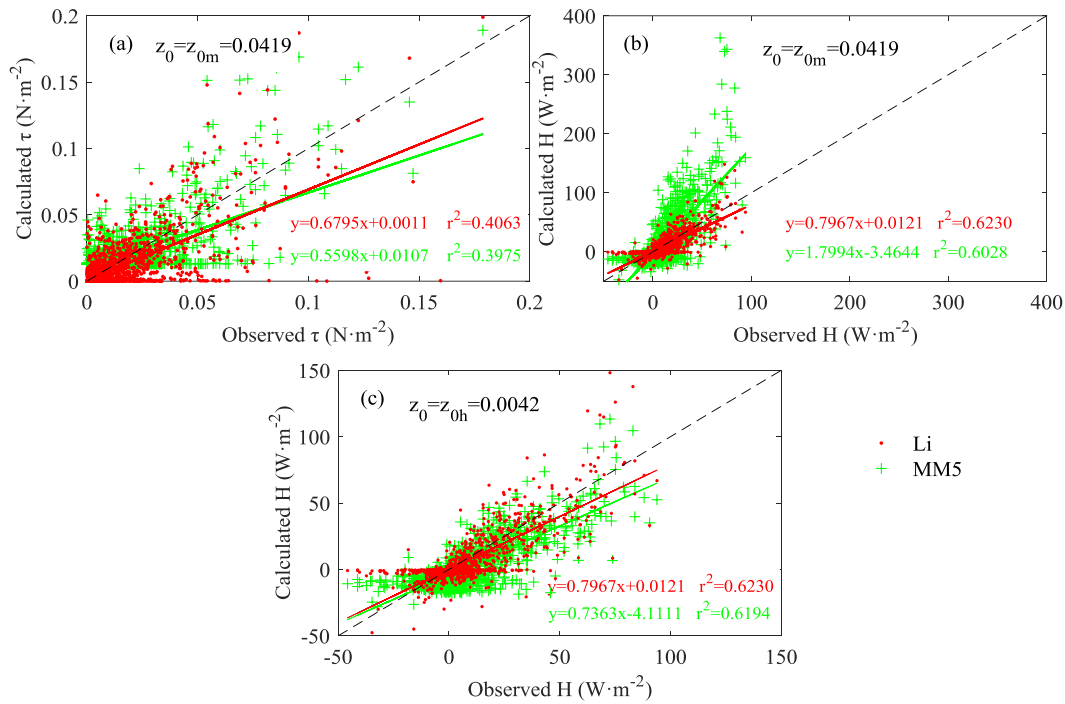
559 **Figure 4.** The relationship between C_M (C_H) and Ri_B for different z_{0m} values and treatment of RSL. Solid lines:
 560 considering the RSL effect; dotted lines: without the RSL effect.

561



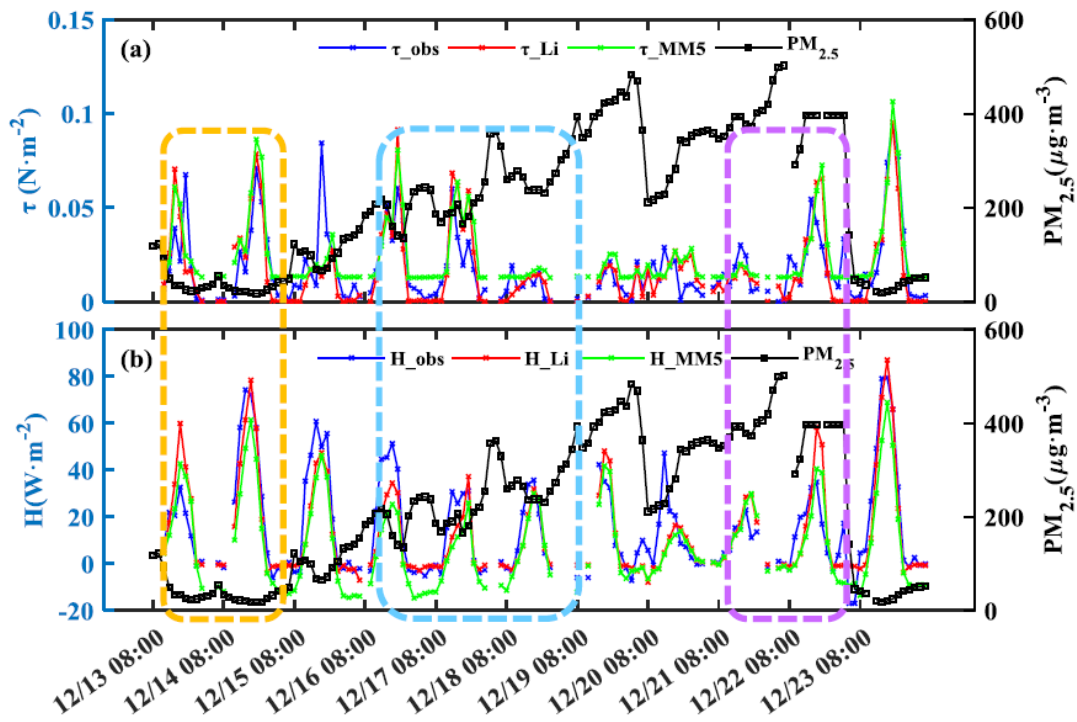
562
563
564
565
566
567

Figure 5. The relationship between C_M (C_H) and Ri_B for different ratios of z_{0m} to z_{0h} and treatment of RSL. Solid lines: considering the RSL effect; dotted lines: without the RSL effect.



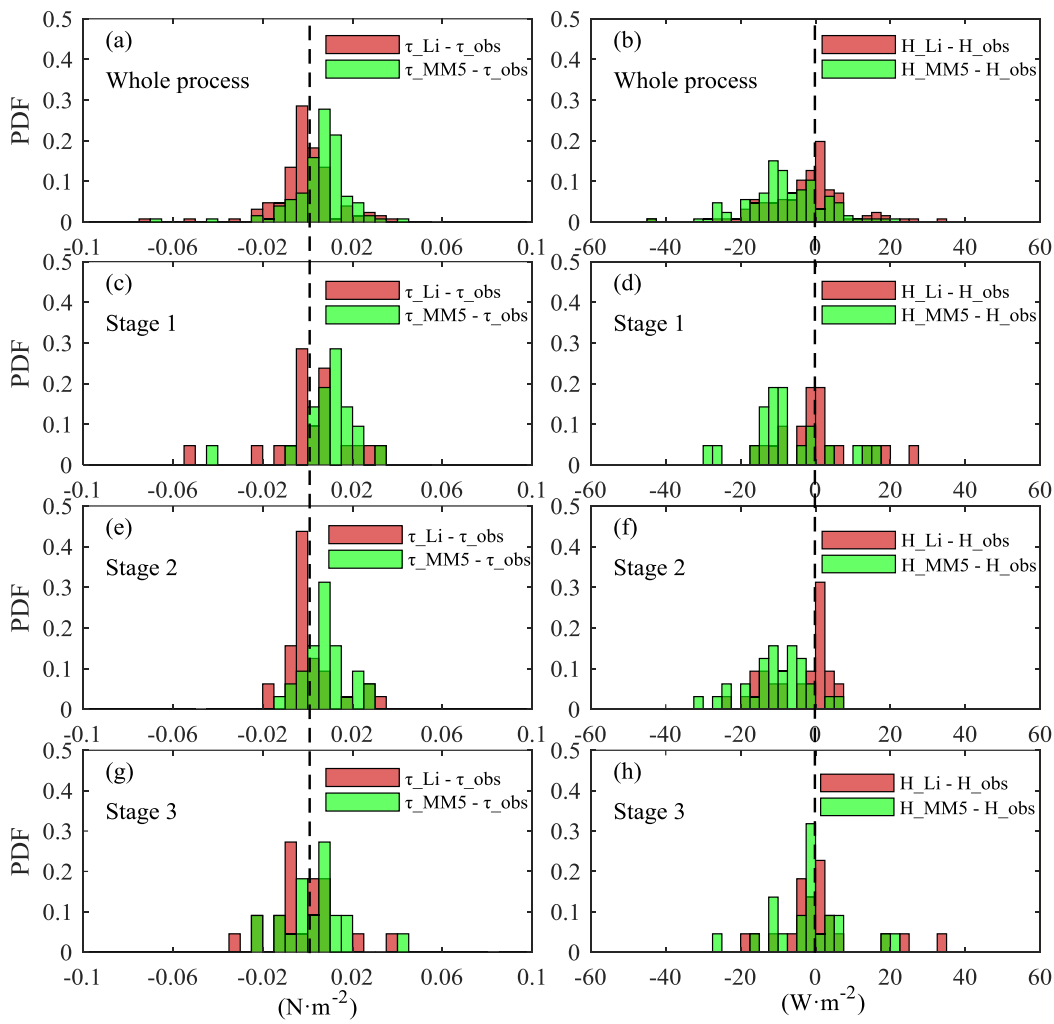
568
569
570
571
572
573
574

Figure 6. Comparison of calculated and observed fluxes at Gucheng station from December 1, 2016 to January 9, 2017. (a) Momentum fluxes (MM5: $z_0 = 0.0419$); (b) sensible heat fluxes (MM5: $z_0 = 0.0419$); (c) sensible heat fluxes (MM5: $z_0 = 0.0042$). Red dots: the Li scheme; green plus signs: the MM5 scheme.



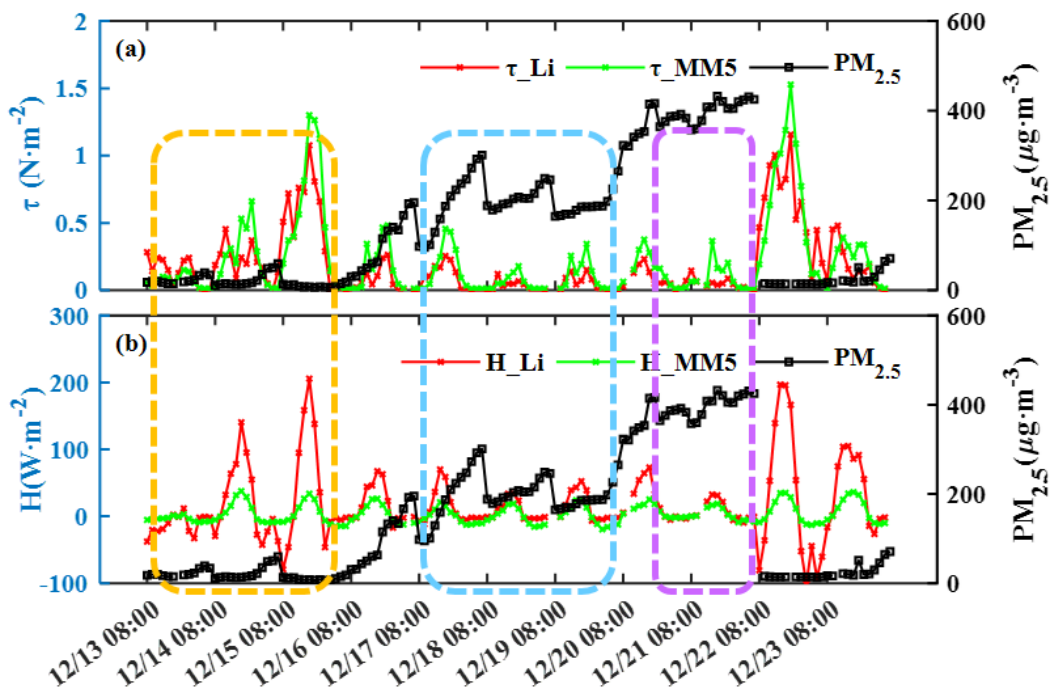
575
576
577
578
579
580
581

Figure 7. Variations of hourly turbulent fluxes and observed $PM_{2.5}$ at Gucheng station in daytime. (a) Momentum fluxes τ (blue line: observations; red line: the Li scheme; green line: the MM5 scheme) and $PM_{2.5}$ concentration (black line); (b) sensible heat fluxes H (the same as τ) and $PM_{2.5}$ concentration (black line). Yellow box: stage 1; blue box: stage 2; purple box: stage 3.



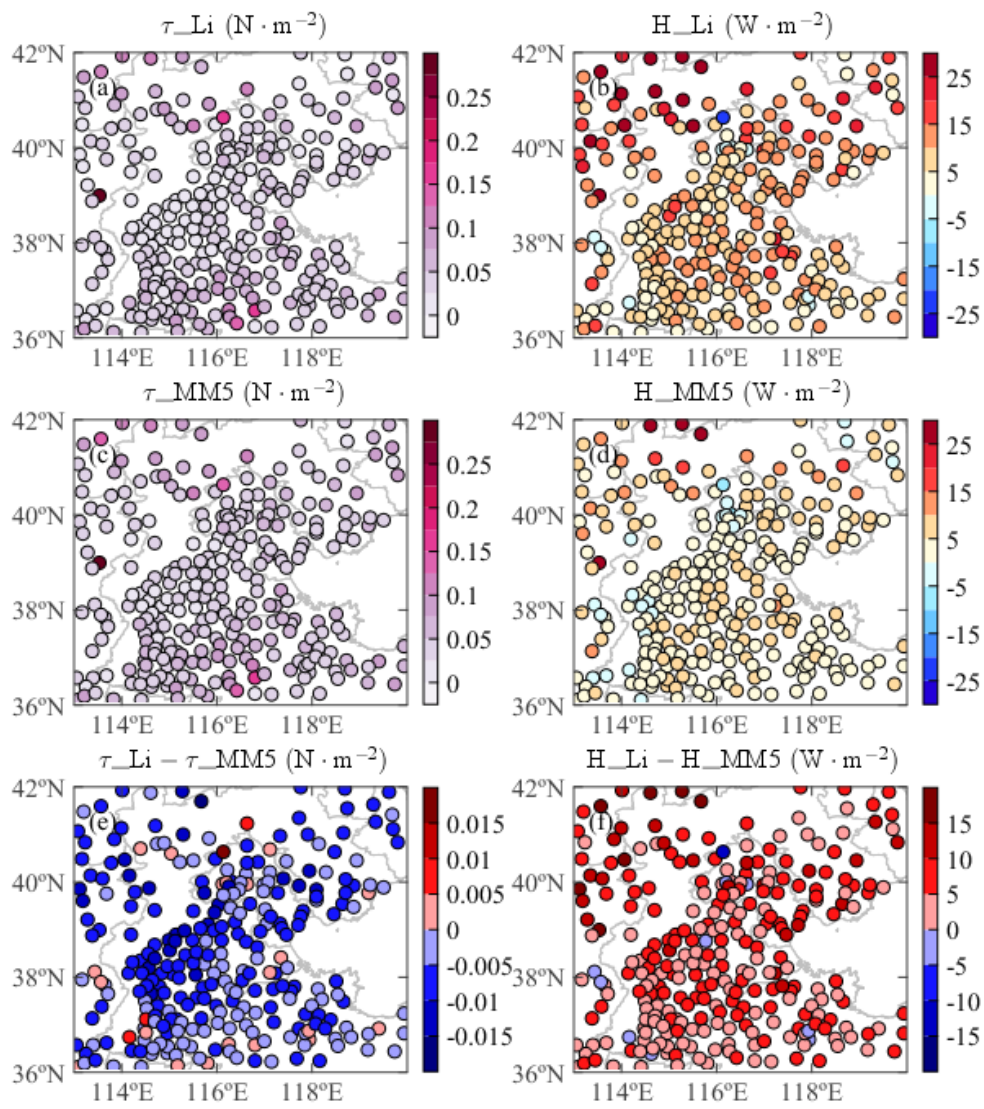
582

583 **Figure 8.** Probability distribution functions (PDF) of the difference between calculated fluxes (momentum fluxes: left;
 584 sensible heat fluxes: right) by using two schemes (the Li scheme: red bars; the MM5 scheme: green bars) and observations in
 585 different stages (a-b: whole process; c-d: stage 1; e-f: stage 2; g-h: stage 3).



586

587 **Figure 9.** As in Fig. 7 but for Beijing station.



589

590 **Figure 10.** The mean momentum and sensible heat fluxes calculated by using two schemes (a-b: the Li scheme; c-d: the
 591 MM5 scheme) and their difference (e: difference of the momentum fluxes; f: difference of the sensible heat fluxes) in
 592 Jing-Jin-Ji during the haze episode (December 13 to 23, 2016).